

MedBridge: Bridging Foundation Vision-Language Models to Medical Image Diagnosis

Yitong Li^{*1,2}, Morteza Ghahremani^{*1,2}, and Christian Wachinger^{1,2}

¹Lab for AI in Medical Imaging, Technical University of Munich (TUM), Germany

²Munich Center for Machine Learning (MCML), Germany

Abstract

Recent vision-language foundation models deliver state-of-the-art results on natural image classification but falter on medical images due to pronounced domain shifts. At the same time, training a medical foundation model requires substantial resources, including extensive annotated data and high computational capacity. To bridge this gap with minimal overhead, we introduce MedBridge, a lightweight multimodal adaptation framework that re-purposes pretrained VLMs for accurate medical image diagnosis. MedBridge comprises three key components. First, a Focal Sampling module that extracts high-resolution local regions to capture subtle pathological features and compensate for the limited input resolution of general-purpose VLMs. Second, a Query Encoder (QEncoder) injects a small set of learnable queries that attend to the frozen feature maps of VLM, aligning them with medical semantics without retraining the entire backbone. Third, a Mixture of Experts mechanism, driven by learnable queries, harnesses the complementary strength of diverse VLMs to maximize diagnostic performance. We evaluate MedBridge on five medical imaging benchmarks across three key adaptation tasks, demonstrating its superior performance in both cross-domain and in-domain adaptation settings, even under varying levels of training data availability. Notably, MedBridge achieved over 6-15% improvement in AUC compared to state-of-the-art VLM adaptation methods in multi-label thoracic disease diagnosis, underscoring its effectiveness in leveraging foundation models for accurate and data-efficient medical diagnosis. Our code is available at <https://github.com/ai-med/MedBridge>.

1 Introduction

Vision-language models (VLMs) have rapidly advanced through large-scale pretraining on extensive datasets that encompass both visual and textual modalities [22; 7; 39; 13]. This pretraining paradigm enables the models to learn rich cross-modal representations, boosting their performance across a variety of downstream tasks [15; 1; 36; 35]. Such tasks include image classification, object detection, and visual grounding, where understanding the semantic relationship between visual content and textual descriptions is crucial. As these foundation models continue to grow in size, full fine-tuning of all parameters for specific applications becomes computationally intensive and elevates the risk of overfitting. Hence, recent research has focused on developing parameter-efficient transfer learning strategies to effectively adapt these large-scale models to downstream tasks across diverse photographic image datasets [48; 38; 47; 50; 6; 8; 37; 9].

Despite these recent advances, adapting general-purpose VLMs to medical imaging remains challenging due to significant domain discrepancies. Medical images are structurally and semantically

^{*}Equal Contribution.

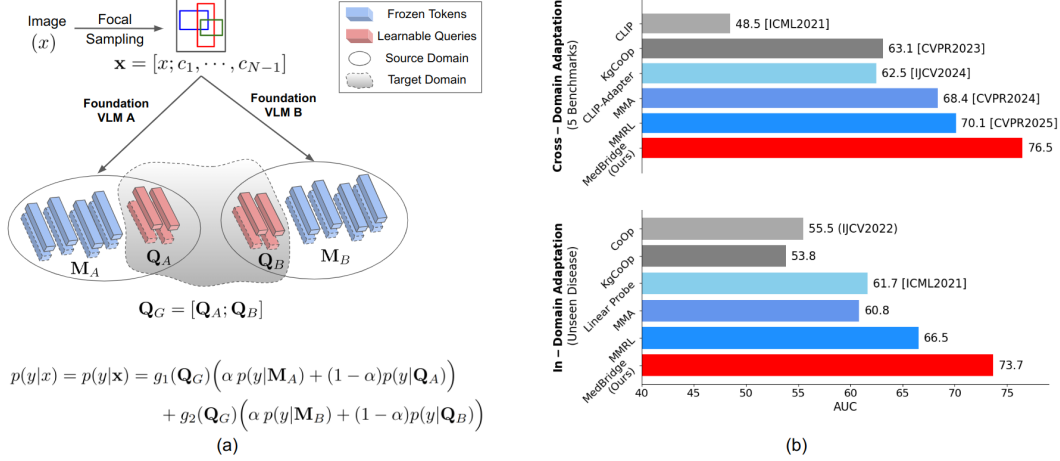


Figure 1: (a) We increase the number of image observations to N via focal sampling. For each observation, we incorporate learnable queries into each expert of the mixture of experts (MoE), where Expert $A : \{\mathbf{M}_A, \mathbf{Q}_A\}$ and Expert $B : \{\mathbf{M}_B, \mathbf{Q}_B\}$. A gating network g , trained on all learnable tokens $\mathbf{Q}_G = [\mathbf{Q}_A, \mathbf{Q}_B]$, dynamically weights the experts, allowing prioritization of different components. The final prediction is a combination of the frozen features \mathbf{M} and the learnable queries \mathbf{Q} , modulated by α . This adds less than 4% parameters compared to the base models. (b) MedBridge yields significant improvements in disease classification across various medical benchmarks. Here, AUC stands for Area Under the Receiver Operating Characteristic Curve.

distinct from natural images: they exhibit subtle pathological features, consistent anatomical layouts, and often require high-resolution input to retain critical pathological details. While natural image tasks rely heavily on high-level object cues, medical diagnosis often hinges on holistic, fine-grained features dispersed across the image. Compounding this issue, the default input resolution of most VLMs (e.g., 224×224) is insufficient to capture the detailed cues in medical images, which typically exceed 2048×2048 pixels. Recent efforts have begun leveraging general-purpose VLMs for medical tasks such as anomaly detection [11; 43], segmentation [20; 44], object detection [21], with promising early results. However, the use of these models for medical image diagnosis, a core clinical task, remains unexplored to the best of our knowledge. Existing VLM adaptation techniques are primarily designed for single-label natural image classification and do not transfer well to medical diagnosis (see Figure 1(b)). The challenge also stems from the multi-label nature of medical diagnosis, where a single image can correspond to multiple co-existing diseases indicated by subtle pathological cues [10].

To address these challenges, we propose MedBridge, an efficient and lightweight framework for adapting foundation VLMs to medical image diagnosis (Figure 1(a)). MedBridge introduces minimal additional parameters, reducing computational overhead and mitigating overfitting risks. It enables effective cross-domain adaptation from general-purpose VLMs and further refinement of medical-pretrained VLMs, maintaining strong performance even with limited training data. Across five benchmark medical datasets for multi-label thoracic disease classification, MedBridge consistently outperforms state-of-the-art adaptation methods, offering substantial clinical advantages through improved accuracy, reduced computational costs, and robust performance under different adaptation scenarios (Figure 1(b)). Our key contributions are:

- A Focal Sampling Module to maintain the high resolution of the original input image on local regions, enabling detection of subtle pathology cues.
- A generic Query Encoder (QEncoder) that bridges the wide domain gap between general-purpose VLMs and medical images with limited learnable queries.
- A Mixture of Experts (MoE) integration on the learnable queries of QEncoders to dynamically combine the strength of multiple foundation VLMs.
- The demonstration of MedBridge’s superior performance for bridging VLMs to the medical domain on five medical datasets and three adaptation tasks.

2 Related Work

Vision-Language Models. Recent VLMs like CLIP [22], ALIGN [13], SigLIP [39], and OpenCLIP [7] have made significant progress by leveraging large-scale contrastive learning on massive datasets with billions of image-text pairs [23], achieving strong performance across diverse downstream tasks. However, their direct deployment in the medical domain remains limited (see Figure 1(b), CLIP) due to a substantial domain shift [27; 24; 46], necessitating further domain-specific adaptation.

Parameter-efficient transfer learning for VLMs. As VLMs scale, fine-tuning all model parameters becomes computationally expensive, prone to overfitting, or catastrophic forgetting. To address this, recent work has focused on parameter-efficient transfer learning, primarily through prompt learning and adapter-based methods. In prompt learning approaches, CoOp [48] replaces fixed templates with learnable vectors, CoCoOp [47] generates instance-specific prompts with visual features, while ProGrad [50] and KgCoOp [38] aim to retain pre-trained knowledge during adaptation. Recent adapter-based methods introduce lightweight modules into the network, in which CLIP-Adapter [8] refines representations using MLP-based adapters, Tip-Adapter [41] enables test-time inference via feature caching, MMA [37] and MMRL [9] both incorporate a shared space to facilitate multimodal interaction. These adaptation strategies are primarily tailored for in-domain, cross-dataset generalization and may not transfer well to cross-domain medical data (see Figure 1(b)). In contrast, with MedBridge we aim to go beyond conventional adapters by explicitly addressing domain discrepancies, enabling robust adaptation from general-purpose VLMs to the medical domain.

Adaptation of general-purpose VLMs to the medical domain. Recent studies have extended pre-trained general-purpose VLMs to domain transfer for report generation [17; 18], anomaly detection [11; 43], segmentation [20; 44], reconstruction [4], and object detection [21] in medical imaging, achieving promising results. However, to the best of our knowledge, the adaptation for medical disease diagnosis is still underexplored. Most current efforts either carry out additional large-scale vision-language pre-training to build medical-specific foundation models [49], e.g., GLORIA [12], ConVIRT [45], MedCLIP [31], CheXzero [27], KAD [42], MedKLIP [32], MGCA [29], MAVL [19], which demands substantial computational resources, or adaptation of VLMs that have already been pre-trained on medical data [24; 40]. In contrast, we aim at a lightweight, flexible adapter to directly re-purpose general-purpose VLMs or further refine medical-pretrained VLMs for unseen disease diagnosis, avoiding the heavy overhead of full re-training while achieving strong clinical performance.

3 Proposed Method

MedBridge is designed as a lightweight adapter to bridge foundation VLMs to the purpose of medical image diagnosis. Let s and t denote the source and target domains, $\{V_s^k\}_{k=1}^K$ being K ViT-based foundation VLM backbones pretrained in the source natural image domain. Our goal is to adapt them for multi-label disease classification on the target medical data $\mathcal{D}_t = \{(x_t^i, y_t^i)\}_{i=1}^{N_t}$, where each image $x_t \in \mathbb{R}^{H \times W \times 3}$ is annotated with ground-truth disease label $y_t \in \{0, 1\}^L$, indicating the presence of L possible diseases: each component $y_{t,j} = 1$ if the j -th disease is present and 0 otherwise, allowing multiple diseases to be indicated simultaneously. y_t will be converted into a list of textual prompts in the template of ‘a radiology image with [CLASS]’, and then encoded by the text encoder of VLM. When paired clinical reports r_t are available, we extend the target set to $\mathcal{D}_t = \{(x_t^i, y_t^i, r_t^i)\}_{i=1}^{N_t}$, incorporating r_t as auxiliary supervision during adaptation. The overall architecture of proposed MedBridge is shown in Figure 2, containing three key modules: 1) a Focal Sampling module extracting high-resolution local regions from original input medical images to capture fine-grained pathological cues and enhance the representation robustness; 2) a Query Encoder (QEncoder) module on top of each VLM encoder, encoding each input into frozen tokens and a small set of learnable queries to enable parameter-efficient domain adaptation; 3) a Mixture of Experts (MoE) module receiving query-augmented tokens and dynamically selecting specialized VLM encoders to improve scalability without computational overhead. The details of each component is provided below.

Focal Sampling: *One image contains the richness of thousands*, especially in medical imaging, where disease manifestations can appear as multiple small and subtle regions, which may vanish when images are down-scaled to the default input size expected by most foundation VLMs. To better preserve detailed pathological cues, we introduce a focal sampling strategy, which augments the resized input image with multiple fine-grained local patches. From each high-resolution input

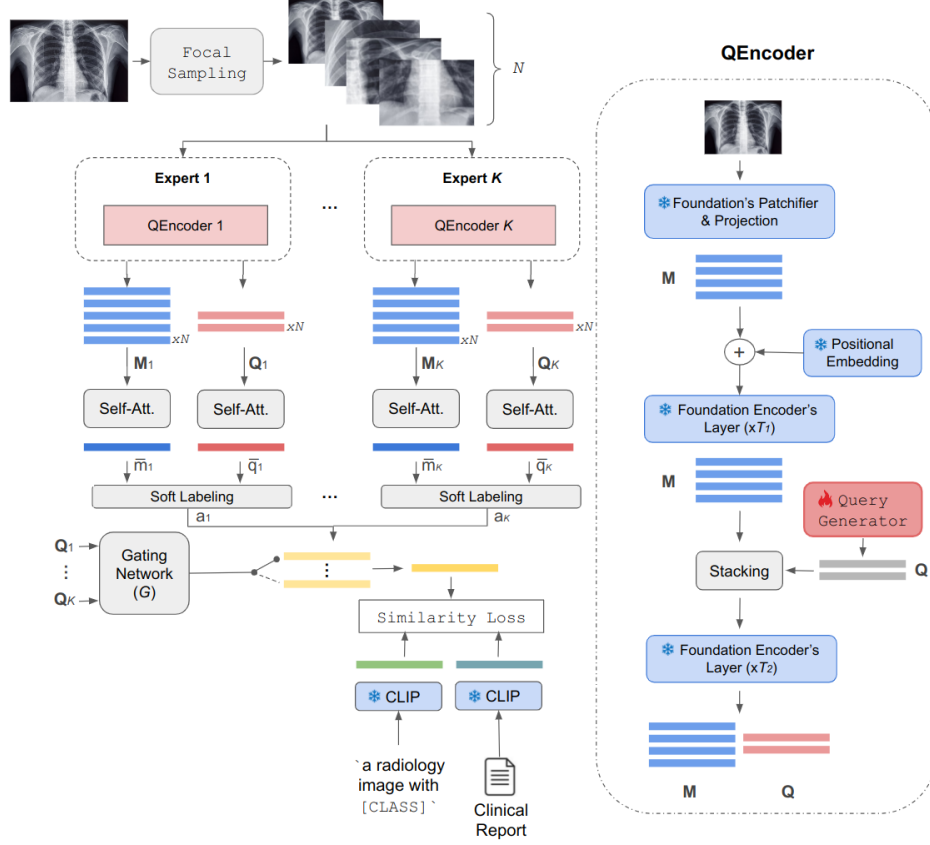


Figure 2: *MedBridge* framework: Focal sampling extracts fine-grained regions from the high-resolution input image, encoded by QEncoders into frozen tokens and learnable queries for lightweight adaptation. A Mixture of Experts (MoE) module routes these tokens through the most relevant encoders, and the final prediction combines soft labels from both query and frozen tokens.

image, we extract $N - 1$ small local regions via either random selection or a sliding window with overlap, and stack them alongside the resized full image to create an N -view input. We later apply self-attention over the N image embeddings to capture their contextual relationships and derive candidate tokens. This strategy enhances the visibility of disease-related regions and reduces the model’s sensitivity to precise image alignments, ensuring more robust detection regardless of slight variations in positioning. It also acts as an implicit ensemble, expanding spatial coverage while mitigating overfitting and overdependence on specific image regions.

Query Encoder (QEncoder): The QEncoder intends to add Q learnable queries $\mathbf{Q} = \{q_i\}_{i=1}^Q$ to interact with the M frozen tokens $\mathbf{M} = \{m_i\}_{i=1}^M$ from foundation VLMs, aiming to reduce the gap in representation between the source and target domains. Due to interactions with the frozen tokens, the auxiliary queries are enriched with contextual content. Concurrently, these auxiliary queries are trained specifically on the target task, enabling them to learn features pertinent to the target domain, while we keep their dimension smaller than the foundation models. As depicted in Figure 2, the QEncoder keeps all T layers of the foundation VLM encoder frozen. After the first T_1 layers, it generates and injects Q learnable query tokens, initialized with a normal distribution $\mathcal{N}(0, 0.02)$, and then stacks them to the foundation feature tokens. The concatenated tokens are processed through the rest T_2 encoder layers ($T_2 = T - T_1$), interacting with each other through attention mapping:

$$\begin{aligned} \mathbf{Z}^i &= [\mathbf{M}^i; \mathbf{Q}^i] + \text{MHSA}(\text{Norm}([\mathbf{M}^i; \mathbf{Q}^i])), \\ [\mathbf{M}^{i+1}; \mathbf{Q}^{i+1}] &= \mathbf{Z}^i + \text{FFN}(\text{Norm}(\mathbf{Z}^i)), \quad i = T_1 + 1, \dots, T, \end{aligned} \quad (1)$$

where MHSA and FFN denote the multi-head self-attention and feed-forward network in the VLM backbones, respectively, and Norm the layer normalization [2]. As each input consists of N associated images after Focal sampling, there exist correspondingly N frozen token sets \mathbf{M} and N trainable query

token sets \mathbf{Q} per model, respectively. We apply a self-attention to extract contextual relationships within N images and then a max-pooling to extract the candidate token, i.e., $\{\bar{m}_k\}_{k=1}^K$ for frozen tokens and $\{\bar{q}_k\}_{k=1}^K$ for learnable query tokens from K expert models. Each model produces an output class token a_k , which is obtained through a softening of the frozen feature and query tokens:

$$a_k = \alpha \bar{m}_k + (1 - \alpha) \bar{q}_k, \quad k = 1, \dots, K, \quad (2)$$

where α is a constant hyperparameter that determines the contribution of the query token set to the resulting class token. An ablation study exploring this hyperparameter is presented in Sec. 4.3.

Mixture of Experts (MoE): The MoE takes the learnable queries $\mathbf{Q}_k \in \mathbb{R}^{N \times Q \times f}$, $k = 1, \dots, K$, where f denotes the embedding dimension, from K expert models as input to a gating network G , which dynamically computes and weights the contribution of each expert. Given an input token set $\mathbf{Q}_G = \{\mathbf{Q}_k\}_{k=1}^K$, the gating network computes a weight vector $\mathbf{g}(\mathbf{Q}_G) = [g_1(\mathbf{Q}_G), g_2(\mathbf{Q}_G), \dots, g_K(\mathbf{Q}_G)]$, where each weight $g_k(\mathbf{Q}_G)$ is obtained via a softmax layer:

$$g_k(\mathbf{Q}_G) = \frac{\exp(\mathbf{w}_k^\top \mathbf{Q}_G + b_k)}{\sum_{j=1}^K \exp(\mathbf{w}_j^\top \mathbf{Q}_G + b_j)}, \quad \sum_{k=1}^K g_k(\mathbf{Q}_G) = 1, \quad g_k(\mathbf{Q}_G) \geq 0, \quad (3)$$

where \mathbf{w}_k and b_k are the learnable parameters of the gating network for the k -th expert. This weighting reflects the relevance of the k -th expert for the input. The final vision embedding output \mathbf{v} is a weighted sum of the outputs from K experts:

$$\mathbf{v} = \sum_{k=1}^K g_k(\mathbf{Q}_G) \cdot a_k. \quad (4)$$

Text Encoding: Given the L possible disease labels, each expressed as a textual prompt in the template of ‘a radiology image with [CLASS]’, we tokenize them and pass them through the frozen text encoder of the foundation VLM. We take the embedding of the end-of-text (EOT) token from the final layer of the text encoder, and project it using a learnable projection layer to align with the vision embedding space, producing L text features $\{\mathbf{z}_l\}_{l=1}^L$. When the paired clinical report r is available, we process it in the same manner as the label textual prompts.

Loss Criterion: Given the vision output $\mathbf{v} \in \mathbb{R}^{1 \times f}$ from the MoE and the textual label features $\{\mathbf{z}_l\}_{l=1}^L$, $\mathbf{z}_l \in \mathbb{R}^{1 \times f}$ for L possible diseases, where f denotes the embedding dimension, we compute the cosine similarity between the given vision output and each label feature via $\text{sim}(\mathbf{v}, \mathbf{z}_l) = \frac{\mathbf{v} \cdot \mathbf{z}_l}{\|\mathbf{v}\| \|\mathbf{z}_l\|}$, where $\|\cdot\|$ represents the L_2 norm. The resulting scores are treated as the predicted logits. Since medical images can be associated with multiple disease labels, we optimize a multi-label binary cross-entropy (BCE) loss, pushing similarities for present disease labels toward 1 and for absent ones toward 0. The same BCE loss is applied between the auxiliary clinical report features (when available) and the textual label features, providing additional supervision during adaptation.

4 Experimental Results

4.1 Experimental Setup

Datasets: We evaluated MedBridge and state-of-the-art adaptation approaches across five distinct medical imaging datasets: MIMIC-CXR v2 [14] ($n = 227k$), CheXpert Plus [3] ($n = 224k$), NIH ChestX-ray14 [30] ($n = 112k$), RSNA Pneumonia [25] ($n = 30k$), and COVIDx CXR-4 [33] ($n = 84k$). MIMIC-CXR, CheXpert Plus, and NIH ChestX-ray14 are multi-label datasets, where each subject may exhibit one or more of 14 common thoracic diseases. In contrast, RSNA Pneumonia consists of binary labels that distinguish normal cases from pneumonia, while COVIDx CXR-4 includes cases labeled either as no findings or COVID-19. Among these, MIMIC-CXR and CheXpert Plus also provide paired radiology reports. Further details are provided in Sec. A.1.

Evaluation metrics: We reported standard metrics for medical image classification: AUC score, macro-averaged F1 score, and accuracy (ACC). The binary decision threshold was chosen to maximize the F1 score, and ACC was also calculated under this threshold. All metrics are macro-averaged over all disease classes present in the target dataset, reported in percentage (%). In addition, we show the computational efficiency of MedBridge and other baselines in Sec. A.3.

Baselines: We compared MedBridge with state-of-the-art adaptation methods for VLMs, including

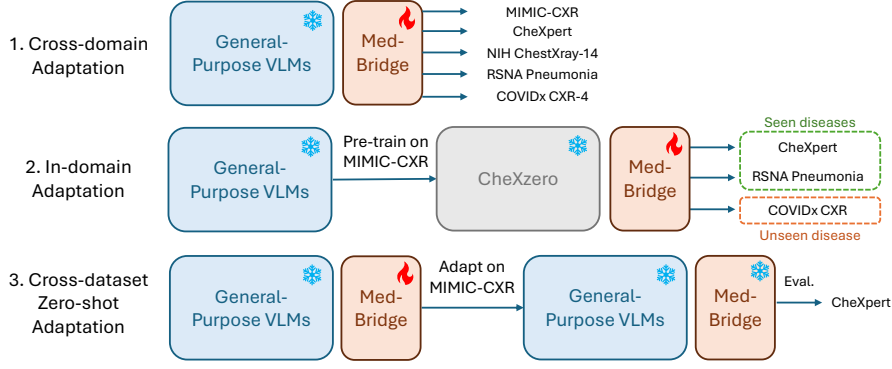


Figure 3: We evaluate MedBridge in three key adaptation tasks: (1) cross-domain adaptation: adapting general-purpose VLMs to medical data; (2) in-domain adaptation: adapting pre-trained medical VLMs to new datasets with seen and unseen diseases, and (3) cross-dataset zero-shot adaptation: after being adapted to a public medical dataset, we test it on a new dataset without further fine-tuning.

the zero-shot baseline with CLIP [22], prompt learning methods: CoOp [48], CoCoOp [47], Pro-Grad [50], KgCoOp [38], adapter-style learning methods: linear probing (LP) [22], CLIP-Adapter [8], MMA [37], MMRL [9], and a medical VLMs adaptation method abbreviated as LP + text [24].

Implementation details: We used the pre-trained CLIP model [22] with a ViT-B/16 backbone and 224×224 input resolution, as the standard general-purpose VLM for adaptation. For other foundation experts, we include SigLIP [39] and an optional vision foundation model Dino-v2 [16]. In the proposed Focal module, local regions were extracted at a size of 512×512 from the full-resolution image and resized to 224×224 as input. We used the AdamW optimizer at a learning rate of 5×10^{-4} and a batch size of 16, training for 3 epochs on a single NVIDIA H100 GPU.

4.2 Evaluation Tasks and Results

To comprehensively assess MedBridge’s adaptation capabilities, we conducted three key evaluations: cross-domain adaptation, in-domain adaptation, and cross-dataset zero-shot adaptation. In cross-domain adaptation, we directly adapted general-purpose VLMs to medical data for disease diagnosis, simulating the challenging task of transferring knowledge from non-medical to medical domains. In in-domain adaptation, we further evaluated how well VLMs, already pre-trained on large-scale medical data (e.g., CheXzero [27]), can adapt to new medical datasets, covering both previously seen and unseen disease scenarios. For both cross- and in-domain adaptation settings, we further assessed performance under varying amounts of labeled training data (1%, 10%, 50%, and 100%) to simulate real-world clinical scenarios with different levels of data availability. Finally, cross-dataset zero-shot adaptation simulates a practical low-resource adaptation scenario: after adapting general-purpose VLMs to the medical domain using a public medical dataset, we directly performed zero-shot multi-label classification on a different dataset without further fine-tuning. Figure 3 visually summarizes these evaluation protocols. Unless stated otherwise, the reported results of MedBridge are without clinical reports or MoE during adaptation to ensure a fair comparison with baseline methods.

4.2.1 Cross-domain Adaptation

In this task, we used public CLIP models pretrained on large-scale natural image-text pairs as representative general-purpose VLMs, and adapted them with MedBridge and state-of-the-art multimodal adaptation approaches on multi-label thoracic disease classification across five medical datasets. As shown in Table 1, zero-shot classification using the pretrained CLIP achieved only around 51% AUC on average, highlighting the significant domain gap between natural and medical images and the need for effective adaptation. Existing adaptation methods substantially improved performance, with MMRL achieving an AUC of 76.46% on CheXpert Plus. MedBridge further boosted accuracy, outperforming MMRL by more than 7% on CheXpert Plus, MIMIC-CXR, and COVIDx CXR-4 datasets, and by approximately 5% on NIH and RSNA Pneumonia, demonstrating its superior generalization and diagnostic performance. The addition of MoE module in MedBridge further enhanced its diagnostic accuracy, especially in CheXpert Plus and COVIDx CXR-4, increasing the AUC by 2% and 2.5% respectively. Integrating auxiliary clinical reports in MIMIC-CXR during adaptation further

Table 1: Evaluation of *cross-domain adaptation* on five medical datasets, in which CheXpert Plus and MIMIC-CXR have paired text reports as auxiliary input.

Method	CheXpert Plus [3]			MIMIC-CXR [14]		
	AUC ↑	F1 ↑	ACC ↑	AUC ↑	F1 ↑	ACC ↑
CLIP (ICML2021) [22]	51.07	28.85	19.65	51.74	22.40	13.46
CoOp (IJCV2022) [48]	66.66	36.72	68.16	63.69	28.57	70.96
CoCoOp (CVPR2022) [47]	61.50	35.03	65.62	59.86	26.97	54.80
ProGrad (ICCV2023) [50]	61.93	35.97	62.02	58.91	26.71	53.51
KgCoOp (CVPR2023) [38]	64.29	35.35	64.51	60.55	27.33	64.53
Linear Probing (ICML2021) [22]	68.45	37.69	71.48	65.20	29.13	68.87
LP + text (MICCAI2024) [24]	51.87	28.85	19.65	53.28	22.40	13.46
CLIP-Adapter (IJCV2024) [8]	62.24	35.11	60.52	57.20	25.93	49.63
MMA (CVPR2024) [37]	74.76	42.98	80.76	64.03	30.16	65.44
MMRL (CVPR2025) [9]	76.46	44.64	80.68	64.74	29.43	65.03
MedBridge	81.49	47.30	<u>85.01</u>	70.59	33.04	76.41
MedBridge (w/ report)	81.69	49.37	85.58	<u>72.01</u>	34.36	77.89
MedBridge (w/ MoE)	83.55	<u>49.94</u>	83.62	71.92	<u>33.95</u>	<u>77.84</u>
MedBridge (w/ report & MoE)	<u>83.28</u>	50.94	82.49	72.03	33.74	77.26

Method	NIH ChestXray-14 [30]			RSNA Pneumonia [25]			COVIDx CXR-4 [33]		
	AUC ↑	F1 ↑	ACC ↑	AUC ↑	F1 ↑	ACC ↑	AUC ↑	F1 ↑	ACC ↑
CLIP [22]	50.11	16.30	9.65	38.98	37.37	22.98	50.74	66.67	50.00
CoOp [48]	57.98	17.78	61.43	82.10	58.38	76.91	56.89	66.77	50.54
CoCoOp [47]	52.12	16.68	36.87	81.58	57.88	76.05	56.16	66.67	50.01
ProGrad [50]	52.89	16.94	38.35	81.23	58.14	77.55	54.18	66.79	50.67
KgCoOp [38]	55.08	17.21	48.76	77.43	54.65	72.94	57.10	66.83	50.85
Linear Probing [22]	58.22	18.45	57.59	81.39	58.00	77.96	58.31	66.91	51.27
LP + text [24]	56.65	16.30	32.65	50.00	37.37	77.02	55.31	66.62	50.00
CLIP-Adapter [8]	51.00	16.68	33.45	78.46	55.08	73.16	58.87	66.69	50.09
MMA [37]	57.83	18.63	47.99	81.86	57.30	76.76	65.06	67.62	53.20
MMRL [9]	60.79	19.42	66.71	82.14	57.67	76.01	66.90	67.92	55.88
MedBridge	<u>65.03</u>	<u>20.86</u>	69.70	<u>85.38</u>	<u>62.08</u>	<u>79.35</u>	<u>73.81</u>	<u>73.22</u>	<u>67.44</u>
MedBridge (w/ MoE)	66.42	22.36	<u>69.58</u>	86.26	62.97	79.50	76.37	75.47	70.51

Table 2: AUC scores (%) of *cross-domain adaptation* under different training data portions.

Task	Cross-domain Adaptation											
Dataset	CheXpert Plus				RSNA Pneumonia				COVIDx CXR-4			
Data Portion	1%	10%	50%	100%	1%	10%	50%	100%	1%	10%	50%	100%
CoOp (IJCV2022)	56.79	65.83	69.95	66.66	74.70	79.04	81.41	82.10	36.15	56.44	58.02	56.89
KgCoOp (CVPR2023)	<u>58.42</u>	57.62	57.78	64.29	62.86	67.74	69.29	77.43	38.44	53.29	54.99	57.10
LP (ICML2021)	58.22	66.30	68.98	68.45	73.01	78.14	80.60	81.39	<u>62.63</u>	59.09	59.51	58.31
MMA (CVPR2024)	49.58	<u>68.96</u>	76.33	74.76	33.05	58.08	81.29	81.86	<u>55.37</u>	<u>61.35</u>	<u>71.68</u>	65.06
MMRL (CVPR2025)	58.71	66.80	<u>76.74</u>	<u>76.46</u>	69.45	74.89	80.03	<u>82.14</u>	58.32	60.59	66.47	<u>66.90</u>
MedBridge (ours)	64.52	69.64	77.22	81.49	76.27	79.84	84.16	85.38	67.75	74.42	76.14	73.81

enhanced its AUC by 1.5%. In addition, as shown in Table 2, MedBridge maintained consistently high performance across different training data proportions, highlighting its strong data efficiency.

4.2.2 In-domain Adaptation

Beyond adapting general-purpose VLMs to the medical domain, we also assessed the ability of MedBridge and other adaptation methods to adapt in-domain pretrained VLMs, i.e., VLMs that have already been further pre-trained on medical datasets, to new medical datasets for diagnosing both previously seen and unseen diseases. To this end, we used CheXzero [27], a self-supervised CLIP-based model pre-trained on the MIMIC-CXR dataset [14]. Since the diseases in CheXpert Plus and RSNA Pneumonia datasets are also present in MIMIC-CXR, we used them to assess in-domain adaptation on seen diseases. In contrast, COVID-19 represents an unseen disease for the CheXzero

Table 3: AUC scores (%) of *in-domain adaptation* under different training data portions.

Task	In-domain Adaptation											
	Seen Diseases								Unseen Disease			
Dataset	CheXpert Plus				RSNA Pneumonia				COVIDx CXR-4			
Data Portion	1%	10%	50%	100%	1%	10%	50%	100%	1%	10%	50%	100%
CoOp (IJCV2022)	58.54	64.95	70.31	72.18	71.37	76.94	79.65	80.52	50.61	55.49	57.68	56.62
KgCoOp (CVPR2023)	59.95	64.11	64.92	64.53	68.34	76.92	77.68	77.66	42.95	53.84	54.39	58.68
LP (ICML2021)	<u>64.38</u>	64.86	74.28	<u>83.30</u>	84.11	86.67	87.69	<u>87.95</u>	60.13	61.66	65.52	65.77
MMA (CVPR2024)	49.25	73.60	<u>77.75</u>	77.96	40.80	81.94	<u>87.55</u>	88.39	50.99	60.84	65.24	69.40
MMRL (CVPR2025)	59.47	69.64	<u>76.57</u>	80.79	74.92	82.55	85.61	85.24	<u>62.64</u>	<u>66.52</u>	<u>67.18</u>	<u>73.49</u>
MedBridge (ours)	68.16	<u>71.53</u>	78.35	86.62	<u>79.73</u>	<u>83.84</u>	86.27	86.32	72.91	73.66	75.26	78.18

model, thus, we utilized the COVIDx CXR-4 dataset to evaluate in-domain adaptation to unseen disease. We also investigated performance under varying amounts of labeled training data. We reported MedBridge with five best-performed adaptation methods here, with full results in Sec. A.2. As Table 3 indicates, in-domain adaptation achieved an overall higher diagnostic accuracy compared to cross-domain adaptation due to the reduced domain gap. Existing adaptation methods performed best for the in-domain adaptation with seen diseases, i.e., CheXpert Plus and RSNA Pneumonia, as they were primarily designed for in-domain use. MedBridge achieved comparably high performance on the seen diseases. Notably, on the unseen disease (COVID-19), MedBridge achieved a significantly higher performance of an AUC score of 78.18%, outperforming the second-best adaptation method by 5%, while maintaining stable results across varying training data proportions. Given the common data scarcity in the medical domain, this setting reflects real-world needs for rapid adaptation to emerging diseases, highlighting the efficiency and practical utility of MedBridge in clinical applications.

4.2.3 Cross-dataset Zero-shot Evaluation

We assessed the cross-dataset adaptation capability of MedBridge by first adapting the general-purpose VLM to the medical domain using the large-scale MIMIC-CXR dataset, aiming to narrow the domain gap between natural and medical images. We then conducted zero-shot multi-label classification on the CheXpert Plus dataset, without further fine-tuning. As presented in Table 4, MedBridge substantially outperformed state-of-the-art adaptation methods, achieving the highest AUC of 79.94%, which is nearly 3.5% higher than the next best method, MMRL. It indicates the effectiveness of MedBridge in improving generalization across diverse medical datasets, showing high potential for real-world clinical deployment, where foundation VLMs can be tuned on public datasets and then reliably deployed in data-limited local clinical settings.

Table 4: Comparisons with SOTA adaptation methods under cross-dataset zero-shot classification.

	Source	Target		
	MIMIC	CheXpert Plus		
	AUC ↑	AUC ↑	F1 ↑	ACC ↑
CoOp [48]	63.69	69.34	38.72	77.15
CoCoOp [47]	59.86	64.81	37.76	70.27
ProGrad [50]	58.91	60.06	34.14	62.80
KgCoOp [38]	60.55	65.29	36.55	72.46
LP [22]	65.20	73.66	40.55	76.31
CLIP-Ad. [8]	57.20	63.92	36.50	71.10
MMA [37]	64.03	76.07	46.84	83.78
MMRL [9]	64.74	76.48	45.20	82.38
MedBridge	70.59	78.69	45.01	84.78
MedB. (w/ MoE)	71.92	79.94	47.15	85.12

4.3 Ablation Study

We performed comprehensive ablation studies to evaluate key designs in MedBridge, including the Focal sampling module, the number of query tokens Q with their weighting factor α , and the MoE module. We reported the average AUC on the validation sets of three representative datasets: CheXpert Plus, MIMIC-CXR, and RSNA Pneumonia, with detailed ablation results provided in Sec. A.4. Additional ablations including the VLM backbones, adapter architecture, and loss weights can be found in Sec. A.5.

Focal sampling: We explored the impact of incorporating varying numbers of fine-grained inputs in our proposed Focal sampling module. To obtain these focal inputs, we evaluated two strategies: randomly sampling the region locations or systematically extracting them using a sliding window with overlap. When the number of desired crops is fewer than the total generated by the sliding

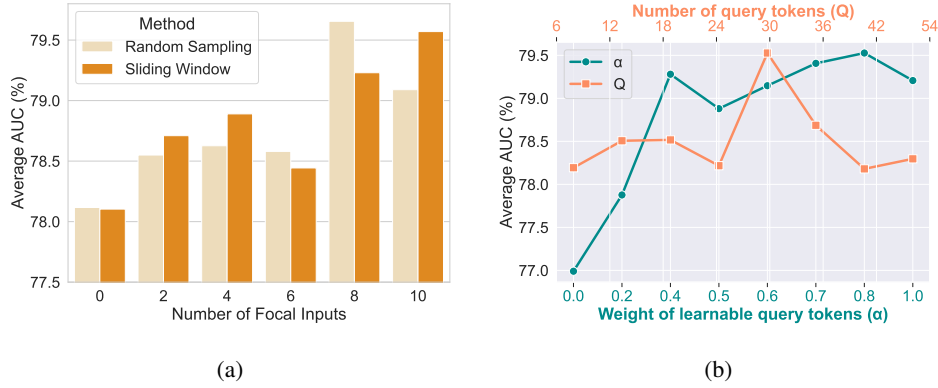


Figure 4: Ablation on (a) the configurations in Focal Sampling, and (b) the weight factor α and the number of learnable query tokens Q .

window, we randomly select a subset. As illustrated in Figure 4a, using only the whole resized image (without fine-grained inputs) resulted in the lowest performance. In contrast, adding more local regions generally led to improved accuracy, and using all those obtained via sliding window yielded the best performance overall. These findings underscore the importance of the proposed Focal module in VLM adaptation to medical imaging: resizing the entire high-resolution medical image to the default input size often leads to the loss of fine-grained pathological details, which are especially critical for detecting diseases manifested in small regions. The Focal sampling module aids in preserving important details while still leveraging the strengths of VLMs for accurate diagnosis.

Weighting factor α and the number of query tokens Q : The constant hyperparameter α controls the contribution of the learnable query tokens generated by the QEncoders in the diagnostic process. We investigated how varying α and the number of learnable query tokens affect adaptation performance, and as shown in Figure 4b, assigning more importance to the query tokens (i.e., using a higher α), and a reasonable number of query tokens, generally led to improved results. This suggests that the learnable query tokens effectively capture rich, task-relevant features that complement the information from the image-text alignment in the VLMs. When α or Q is low, the model likely underutilizes these task-adaptive representations, relying more on the global or fixed representations from the foundation model, which may not sufficiently capture the pathology-specific cues for medical diagnosis. However, it is also important to balance this contribution, as excessively high values of α or Q could lead to overfitting to the query space or diminish the benefits of pre-trained knowledge. Overall, these results validate the effectiveness of incorporating learnable, task-specific representations through the proposed QEncoders.

Mixture of Experts (MoE): We evaluated the impact of MoE module and the integration of different foundation models for disease diagnosis. The foundation models evaluated include CLIP [22], SigLIP [39], DINOv2 [16], EVA-CLIP [26], and MetaCLIP [34]. SigLIP [39] leverages a pairwise sigmoid loss for language-image pre-training. We used the SigLIP 2 vision-language model [28] pre-trained on the WebLI dataset [5] containing 10 billion images and 12 billion alt-texts covering 109 languages. DINOv2 [16] is a vision foundation model pre-trained in a self-supervised manner using the LVD-142M dataset. EVA-CLIP [26] incorporates several techniques that can significantly reduce training costs, stabilize the training process, and improve zero-shot performance compared to the original CLIP model. The model is pre-trained on ImageNet-22k with masked image modeling and fine-tuned on ImageNet-22k by the paper authors. MetaCLIP [34], the Metadata-Curated Language-Image Pre-training, takes a raw data pool and metadata (derived from CLIP’s concepts) and yields a balanced subset over the metadata distribution. The model is pre-trained on 2.5 billion image-text pairs. We evaluated the performance of MedBridge using different combinations of the available experts. As shown in Table 5, using CLIP alone provided a baseline with an AUC of 85.08% in RSNA Pneumonia and 75.41% in CheXpert Plus, and adding a second expert, especially EVA-CLIP and MetaCLIP, substantially improved the performance in both datasets, resulting in an AUC of 78.53% in CheXpert Plus using both CLIP and MetaCLIP. The full mixture of all five experts achieved the best AUC score of 86.81% in RSNA Pneumonia and 79.37% in CheXpert Plus. Certain three- and four-expert combinations, such as CLIP + DINOv2 + EVA-CLIP + MetaCLIP, also performed competitively, which reached the highest accuracy of 83.21% in RSNA Pneumonia. These results confirm that leveraging diverse expert foundation models allows MedBridge to capture complementary visual representations, leading to improved diagnostic performance.

Table 5: MedBridge performance with different mixtures of experts.

Experts					RSNA Pneumonia		CheXpert Plus	
CLIP	SigLIP	DINOv2	EVA-CLIP	MetaCLIP	AUC \uparrow	ACC \uparrow	AUC \uparrow	ACC \uparrow
✓					85.08	78.31	75.41	75.64
✓	✓				85.98	79.20	76.25	77.48
✓		✓			85.62	82.17	76.81	75.92
✓			✓		86.66	82.13	76.87	77.86
✓				✓	86.27	81.49	78.53	78.82
✓	✓	✓			86.26	82.84	76.44	76.27
✓		✓		✓	86.72	82.50	77.48	78.22
✓		✓	✓	✓	86.61	83.21	76.92	75.64
✓	✓	✓	✓	✓	86.81	82.47	79.37	77.19

5 Discussion and Conclusion

We introduced MedBridge, a lightweight and effective adapter designed to enhance the adaptation of general-purpose VLMs for medical image diagnosis. MedBridge introduces a Focal sampling module tailored to grasp fine-grained features in medical imaging, a novel QEncoder module with learnable query tokens to obtain domain-specific features, and an MoE mechanism to better leverage the diverse capabilities of foundation VLMs. While medical vision-language pretraining typically takes several days on multiple GPUs [27], MedBridge completes adaptation in just a few hours using one single GPU (See Sec. A.3). It proves effective in three key evaluations: cross-domain adaptation, in-domain adaptation, cross-dataset zero-shot transfer, and remains robust even with limited labeled training data. Across five public medical datasets, MedBridge consistently outperforms existing adaptation strategies in accuracy, data efficiency, and generalization. This performance gain is largely due to its effective use of learnable query tokens and expert foundation models with the capability to capture pathological cues from fine-grained regions. One limitation is its increased training time in comparison to other adapters, incurred by adding multiple experts and the Focal Sampling module. Yet, this is still only a fraction of the required resources for original VLM training.

Broader Impact: MedBridge’s lightweight adaptation framework lowers the barriers to deploying AI-driven diagnostic tools in resource-constrained regions by reducing computational and data requirements. At the same time, robust oversight policies need to be established to guard against over-reliance on AI assistance and subsequent clinician de-skilling.

Acknowledgements

This work was supported by the Munich Center for Machine Learning (MCML) and the German Research Foundation (DFG). The authors gratefully acknowledge the computational and data resources provided by the Leibniz Supercomputing Centre.

References

- [1] A. Awadalla, I. Gao, J. Gardner, J. Hessel, Y. Hanafy, W. Zhu, K. Marathe, Y. Bitton, S. Gadre, S. Sagawa, et al. Openflamingo: An open-source framework for training large autoregressive vision-language models. *arXiv preprint arXiv:2308.01390*, 2023.
- [2] J. L. Ba, J. R. Kiros, and G. E. Hinton. Layer normalization. *arXiv preprint arXiv:1607.06450*, 2016.
- [3] P. Chambon, J.-B. Delbrouck, T. Sounack, S.-C. Huang, Z. Chen, M. Varma, S. Q. Truong, C. T. Chuong, and C. P. Langlotz. Chexpert plus: Augmenting a large chest x-ray dataset with text radiology reports, patient demographics and additional image formats. *arXiv preprint arXiv:2405.19538*, 2024.
- [4] P. J. M. Chambon, C. Bluethgen, C. Langlotz, and A. Chaudhari. Adapting pretrained vision-language foundational models to medical imaging domains. In *NeurIPS 2022 Foundation Models for Decision Making Workshop*.
- [5] X. Chen, X. Wang, S. Changpinyo, A. Piergiovanni, P. Padlewski, D. Salz, S. Goodman, A. Grycner, B. Mustafa, L. Beyer, et al. Pali: A jointly-scaled multilingual language-image model. In *The Eleventh International Conference on Learning Representations*, 2023.
- [6] C. Cheng, L. Song, R. Xue, H. Wang, H. Sun, Y. Ge, and Y. Shan. Meta-adapter: an online few-shot learner for vision-language model. In *Proceedings of the 37th International Conference on Neural Information Processing Systems*, pages 55361–55374, 2023.
- [7] M. Cherti, R. Beaumont, R. Wightman, M. Wortsman, G. Ilharco, C. Gordon, C. Schuhmann, L. Schmidt, and J. Jitsev. Reproducible scaling laws for contrastive language-image learning. In *Proceedings of the IEEE/CVF conference on computer vision and pattern recognition*, pages 2818–2829, 2023.
- [8] P. Gao, S. Geng, R. Zhang, T. Ma, R. Fang, Y. Zhang, H. Li, and Y. Qiao. Clip-adapter: Better vision-language models with feature adapters. *International Journal of Computer Vision*, 132(2):581–595, 2024.
- [9] Y. Guo and X. Gu. Mmrl: Multi-modal representation learning for vision-language models. In *Proceedings of the IEEE/CVF Conference on Computer Vision and Pattern Recognition*, 2025.
- [10] G. Holste, Y. Zhou, S. Wang, A. Jaiswal, M. Lin, S. Zhuge, Y. Yang, D. Kim, T.-H. Nguyen-Mau, M.-T. Tran, et al. Towards long-tailed, multi-label disease classification from chest x-ray: Overview of the cxr-1t challenge. *Medical Image Analysis*, page 103224, 2024.
- [11] C. Huang, A. Jiang, J. Feng, Y. Zhang, X. Wang, and Y. Wang. Adapting visual-language models for generalizable anomaly detection in medical images. In *Proceedings of the IEEE/CVF Conference on Computer Vision and Pattern Recognition*, pages 11375–11385, 2024.
- [12] S.-C. Huang, L. Shen, M. P. Lungren, and S. Yeung. Gloria: A multimodal global-local representation learning framework for label-efficient medical image recognition. In *Proceedings of the IEEE/CVF international conference on computer vision*, pages 3942–3951, 2021.
- [13] C. Jia, Y. Yang, Y. Xia, Y.-T. Chen, Z. Parekh, H. Pham, Q. Le, Y.-H. Sung, Z. Li, and T. Duerig. Scaling up visual and vision-language representation learning with noisy text supervision. In M. Meila and T. Zhang, editors, *Proceedings of the 38th International Conference on Machine Learning*, volume 139 of *Proceedings of Machine Learning Research*, pages 4904–4916. PMLR, 18–24 Jul 2021.
- [14] A. E. Johnson, T. J. Pollard, S. J. Berkowitz, N. R. Greenbaum, M. P. Lungren, C.-y. Deng, R. G. Mark, and S. Horng. MIMIC-CXR, a de-identified publicly available database of chest radiographs with free-text reports. *Scientific data*, 6(1):317, 2019.
- [15] A. Liu, B. Feng, B. Xue, B. Wang, B. Wu, C. Lu, C. Zhao, C. Deng, C. Zhang, C. Ruan, et al. Deepseek-v3 technical report. *arXiv preprint arXiv:2412.19437*, 2024.
- [16] M. Oquab, T. Darcet, T. Moutakanni, H. V. Vo, M. Szafraniec, V. Khalidov, P. Fernandez, D. HAZIZA, F. Massa, A. El-Nouby, et al. DINOv2: Learning robust visual features without supervision. *Transactions on Machine Learning Research*, 2024.
- [17] C. Pellegrini, E. Özsoy, B. Busam, B. Wiestler, N. Navab, and M. Keicher. Radialog: Large vision-language models for x-ray reporting and dialog-driven assistance. In *Medical Imaging with Deep Learning*, 2025.
- [18] F. Pérez-García, H. Sharma, S. Bond-Taylor, K. Bouzid, V. Salvatelli, M. Ilse, S. Bannur, D. C. Castro, A. Schwaighofer, M. P. Lungren, et al. Exploring scalable medical image encoders beyond text supervision. *Nature Machine Intelligence*, pages 1–12, 2025.

- [19] V. M. H. Phan, Y. Xie, Y. Qi, L. Liu, L. Liu, B. Zhang, Z. Liao, Q. Wu, M.-S. To, and J. W. Verjans. Decomposing disease descriptions for enhanced pathology detection: A multi-aspect vision-language pre-training framework. In *Proceedings of the IEEE/CVF Conference on Computer Vision and Pattern Recognition*, pages 11492–11501, 2024.
- [20] K. Poudel, M. Dhakal, P. Bhandari, R. Adhikari, S. Thapaliya, and B. Khanal. Exploring transfer learning in medical image segmentation using vision-language models. In *Medical Imaging with Deep Learning*, pages 1142–1165. PMLR, 2024.
- [21] Z. Qin, H. Yi, Q. Lao, and K. Li. Medical image understanding with pretrained vision language models: A comprehensive study. In *The Eleventh International Conference on Learning Representations*.
- [22] A. Radford, J. W. Kim, C. Hallacy, A. Ramesh, G. Goh, S. Agarwal, G. Sastry, A. Askell, P. Mishkin, J. Clark, et al. Learning transferable visual models from natural language supervision. In *International conference on machine learning*, pages 8748–8763. PmLR, 2021.
- [23] C. Schuhmann, R. Beaumont, R. Vencu, C. Gordon, R. Wightman, M. Cherti, T. Coombes, A. Katta, C. Mullis, M. Wortsman, et al. Laion-5b: An open large-scale dataset for training next generation image-text models. *Advances in neural information processing systems*, 35:25278–25294, 2022.
- [24] F. Shakeri, Y. Huang, J. Silva-Rodríguez, H. Bahig, A. Tang, J. Dolz, and I. Ben Ayed. Few-shot adaptation of medical vision-language models. In *International Conference on Medical Image Computing and Computer-Assisted Intervention*, pages 553–563. Springer, 2024.
- [25] G. Shih, C. C. Wu, S. S. Halabi, M. D. Kohli, L. M. Prevedello, T. S. Cook, A. Sharma, J. K. Amorosa, V. Arteaga, M. Galperin-Aizenberg, et al. Augmenting the national institutes of health chest radiograph dataset with expert annotations of possible pneumonia. *Radiology: Artificial Intelligence*, 1(1):e180041, 2019.
- [26] Q. Sun, Y. Fang, L. Wu, X. Wang, and Y. Cao. Eva-clip: Improved training techniques for clip at scale. *arXiv preprint arXiv:2303.15389*, 2023.
- [27] E. Tiu, E. Talius, P. Patel, C. P. Langlotz, A. Y. Ng, and P. Rajpurkar. Expert-level detection of pathologies from unannotated chest x-ray images via self-supervised learning. *Nature biomedical engineering*, 6(12): 1399–1406, 2022.
- [28] M. Tschannen, A. Gritsenko, X. Wang, M. F. Naeem, I. Alabdulmohsin, N. Parthasarathy, T. Evans, L. Beyer, Y. Xia, B. Mustafa, et al. Siglip 2: Multilingual vision-language encoders with improved semantic understanding, localization, and dense features. *arXiv preprint arXiv:2502.14786*, 2025.
- [29] F. Wang, Y. Zhou, S. Wang, V. Vardhanabhuti, and L. Yu. Multi-granularity cross-modal alignment for generalized medical visual representation learning. *Advances in Neural Information Processing Systems*, 35:33536–33549, 2022.
- [30] X. Wang, Y. Peng, L. Lu, Z. Lu, M. Bagheri, and R. M. Summers. Chestx-ray8: Hospital-scale chest x-ray database and benchmarks on weakly-supervised classification and localization of common thorax diseases. In *Proceedings of the IEEE conference on computer vision and pattern recognition*, pages 2097–2106, 2017.
- [31] Z. Wang, Z. Wu, D. Agarwal, and J. Sun. Medclip: Contrastive learning from unpaired medical images and text. In *Proceedings of the Conference on Empirical Methods in Natural Language Processing. Conference on Empirical Methods in Natural Language Processing*, volume 2022, page 3876, 2022.
- [32] C. Wu, X. Zhang, Y. Zhang, Y. Wang, and W. Xie. Medklip: Medical knowledge enhanced language-image pre-training for x-ray diagnosis. In *Proceedings of the IEEE/CVF International Conference on Computer Vision*, pages 21372–21383, 2023.
- [33] Y. Wu, H. Gunraj, C.-e. A. Tai, and A. Wong. Covidx cxr-4: An expanded multi-institutional open-source benchmark dataset for chest x-ray image-based computer-aided covid-19 diagnostics. *arXiv preprint arXiv:2311.17677*, 2023.
- [34] H. Xu, S. Xie, X. Tan, P.-Y. Huang, R. Howes, V. Sharma, S.-W. Li, G. Ghosh, L. Zettlemoyer, and C. Feichtenhofer. Demystifying clip data. In *The Twelfth International Conference on Learning Representations*, 2024.
- [35] S. Yamaguchi, D. Feng, S. Kanai, K. Adachi, and D. Chijiwa. Post-pre-training for modality alignment in vision-language foundation models. In *Proceedings of the IEEE/CVF Conference on Computer Vision and Pattern Recognition*, 2025.

- [36] A. Yang, B. Yang, B. Zhang, B. Hui, B. Zheng, B. Yu, C. Li, D. Liu, F. Huang, H. Wei, et al. Qwen2. 5 technical report. *arXiv preprint arXiv:2412.15115*, 2024.
- [37] L. Yang, R.-Y. Zhang, Y. Wang, and X. Xie. Mma: Multi-modal adapter for vision-language models. In *Proceedings of the IEEE/CVF Conference on Computer Vision and Pattern Recognition*, pages 23826–23837, 2024.
- [38] H. Yao, R. Zhang, and C. Xu. Visual-language prompt tuning with knowledge-guided context optimization. In *Proceedings of the IEEE/CVF conference on computer vision and pattern recognition*, pages 6757–6767, 2023.
- [39] X. Zhai, B. Mustafa, A. Kolesnikov, and L. Beyer. Sigmoid loss for language image pre-training. In *Proceedings of the IEEE/CVF international conference on computer vision*, pages 11975–11986, 2023.
- [40] J. Zhang, G. Wang, M. K. Kalra, and P. Yan. Disease-informed adaptation of vision-language models. *IEEE Transactions on Medical Imaging*, 2024.
- [41] R. Zhang, W. Zhang, R. Fang, P. Gao, K. Li, J. Dai, Y. Qiao, and H. Li. Tip-adapter: Training-free adaption of clip for few-shot classification. In *Computer Vision – ECCV 2022: 17th European Conference, Tel Aviv, Israel, October 23–27, 2022, Proceedings, Part XXXV*, page 493–510. Springer-Verlag, 2022. ISBN 978-3-031-19832-8. doi: 10.1007/978-3-031-19833-5_29.
- [42] X. Zhang, C. Wu, Y. Zhang, W. Xie, and Y. Wang. Knowledge-enhanced visual-language pre-training on chest radiology images. *Nature Communications*, 14(1):4542, 2023.
- [43] X. Zhang, M. Xu, D. Qiu, R. Yan, N. Lang, and X. Zhou. Medclip: Adapting clip for few-shot medical image anomaly detection. In *International Conference on Medical Image Computing and Computer-Assisted Intervention*, pages 458–468. Springer, 2024.
- [44] Y. Zhang, S.-C. Huang, Z. Zhou, M. P. Lungren, and S. Yeung. Adapting pre-trained vision transformers from 2d to 3d through weight inflation improves medical image segmentation. In *Machine Learning for Health*, pages 391–404. PMLR, 2022.
- [45] Y. Zhang, H. Jiang, Y. Miura, C. D. Manning, and C. P. Langlotz. Contrastive learning of medical visual representations from paired images and text. In *Machine learning for healthcare conference*, pages 2–25. PMLR, 2022.
- [46] Z. Zhao, Y. Liu, H. Wu, M. Wang, Y. Li, S. Wang, L. Teng, D. Liu, Z. Cui, Q. Wang, et al. Clip in medical imaging: A survey. *Medical Image Analysis*, page 103551, 2025.
- [47] K. Zhou, J. Yang, C. C. Loy, and Z. Liu. Conditional prompt learning for vision-language models. In *Proceedings of the IEEE/CVF conference on computer vision and pattern recognition*, pages 16816–16825, 2022.
- [48] K. Zhou, J. Yang, C. C. Loy, and Z. Liu. Learning to prompt for vision-language models. *International Journal of Computer Vision*, 130(9):2337–2348, 2022.
- [49] Y. Zhou, T. Faith, Y. Xu, S. Leng, X. Xu, Y. Liu, and R. S. M. Goh. Benchx: A unified benchmark framework for medical vision-language pretraining on chest x-rays. *Advances in Neural Information Processing Systems*, 37:6625–6647, 2024.
- [50] B. Zhu, Y. Niu, Y. Han, Y. Wu, and H. Zhang. Prompt-aligned gradient for prompt tuning. In *Proceedings of the IEEE/CVF international conference on computer vision*, pages 15659–15669, 2023.